

Supporting Information

Hierarchical Nanoclusters with Programmed Disassembly for Mitochondria-targeted Tumor Therapy with MR imaging

Congkun Xie ^{1,□}, Dong Cen ^{2,□}, Huiyang Wang ², Yifan Wang ², Yongjun Wu ¹, Gaorong Han ¹, Xiang Li ^{1,3*}

¹ State Key Laboratory of Silicon Materials, School of Materials Science and Engineering, Zhejiang University, Hangzhou, Zhejiang 310027, P. R. China

² Key Laboratory of Endoscopic Technique Research of Zhejiang Province, Sir Run Run Shaw Hospital, Zhejiang University, Hangzhou 215123, P. R. China

³ ZJU-Hangzhou Global Scientific and Technological Innovation Center, Zhejiang University, Hangzhou, 311200, P.R. China.

* Corresponding Author: xiang.li@zju.edu.cn (XL)

□ Authors with equal contribution

Supporting Figures

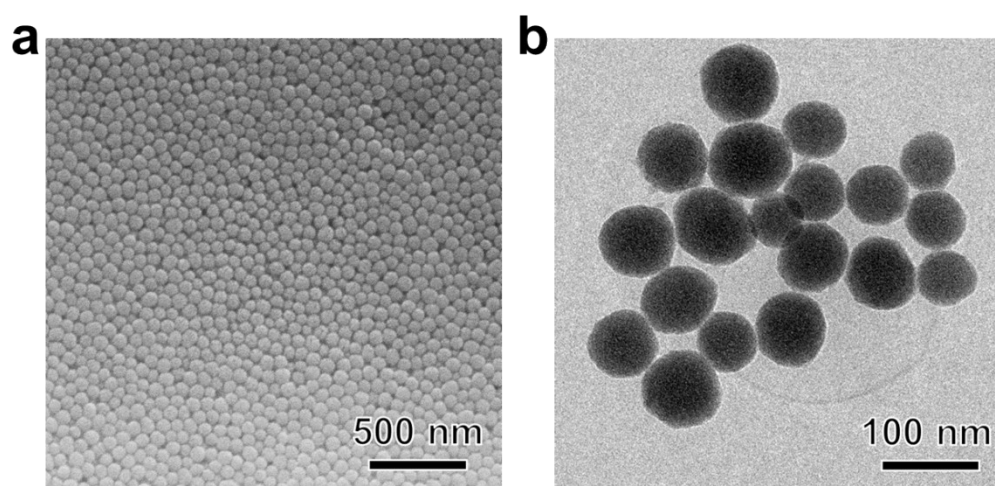


Figure S1. (a) SEM and (b) TEM images of SiO₂ nanoparticles precursor.

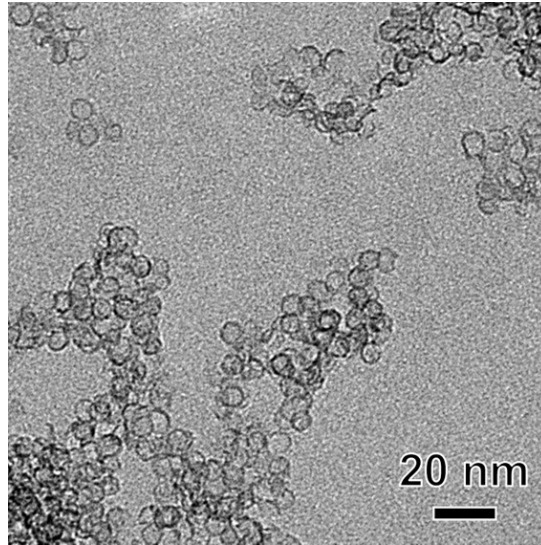


Figure S2. Manganese silicate nanocapsules prepared by using disodium maleate and potassium permanganate as precursors.

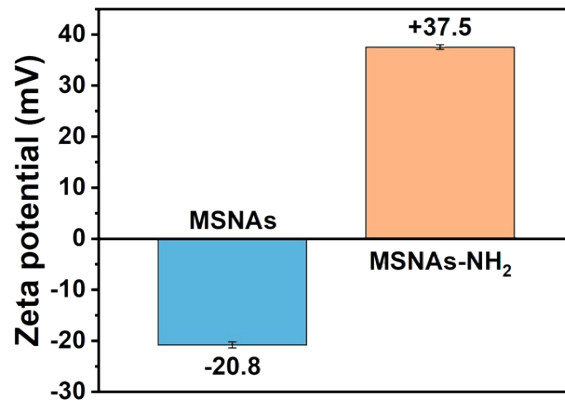


Figure S3. Zeta potentials of MSNAs before and after PEI modification.

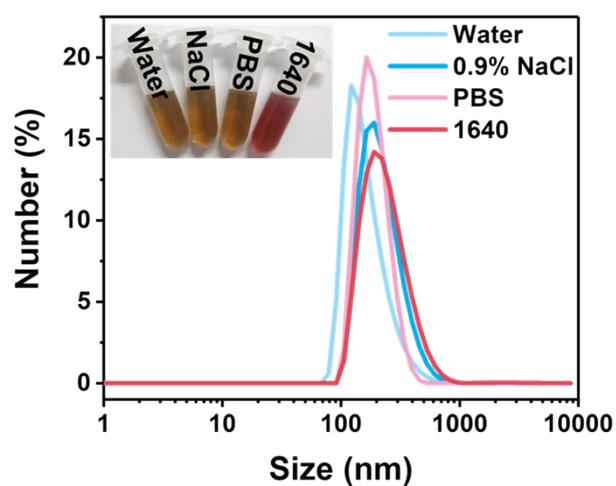


Figure S4. Dynamic light scattering (DLS) profiles and optical images of MSNAs-TPP in pure water, normal saline, PBS, and RPMI-1640 cell culture medium.

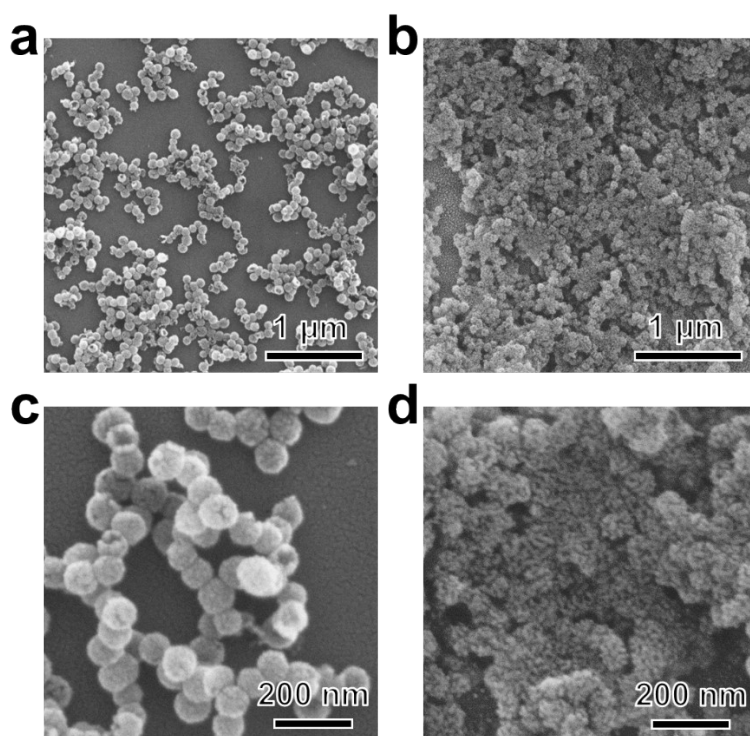


Figure S5. SEM images of MSNAs-TPP (a), (c) before and (b), (d) after the acid treatment at different magnifications.

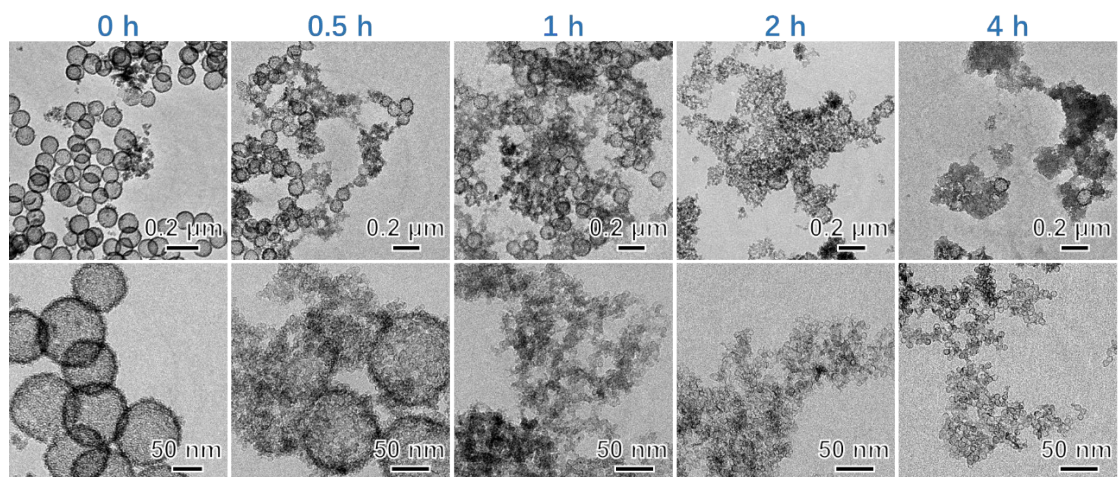


Figure S6. TEM observations of MSNAs-TPP structure evolution in pH 6.5 over time at varied magnifications.

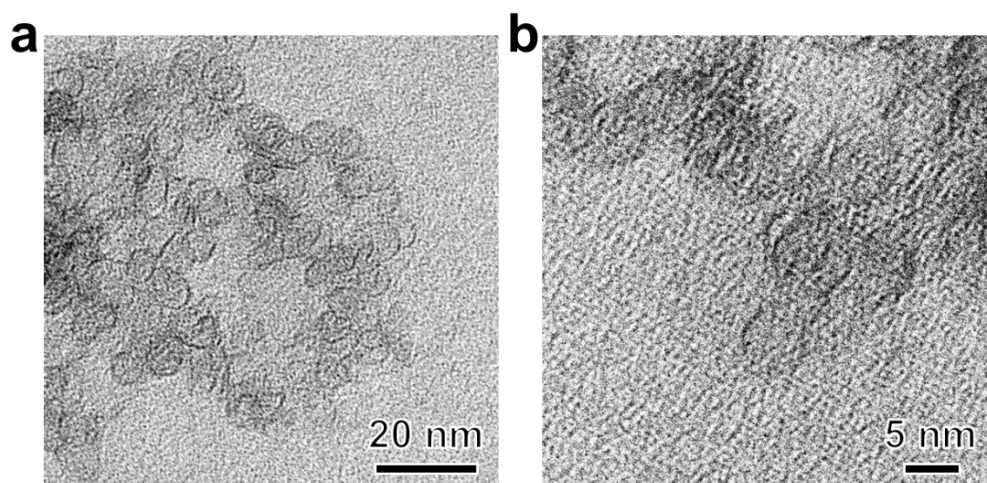


Figure S7. High resolution TEM images of disassembled nanocapsules.

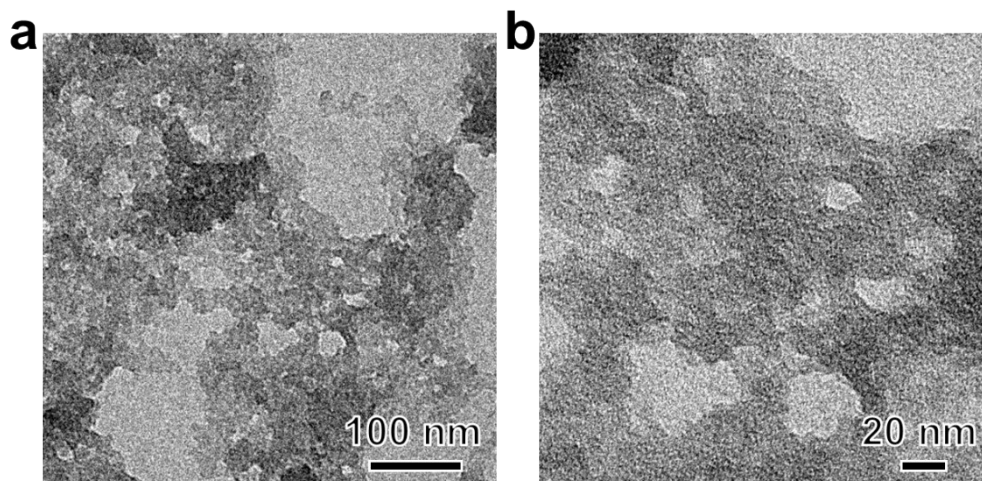


Figure S8. TEM images of MSNAs-TPP degraded in 10 mM GSH solution.

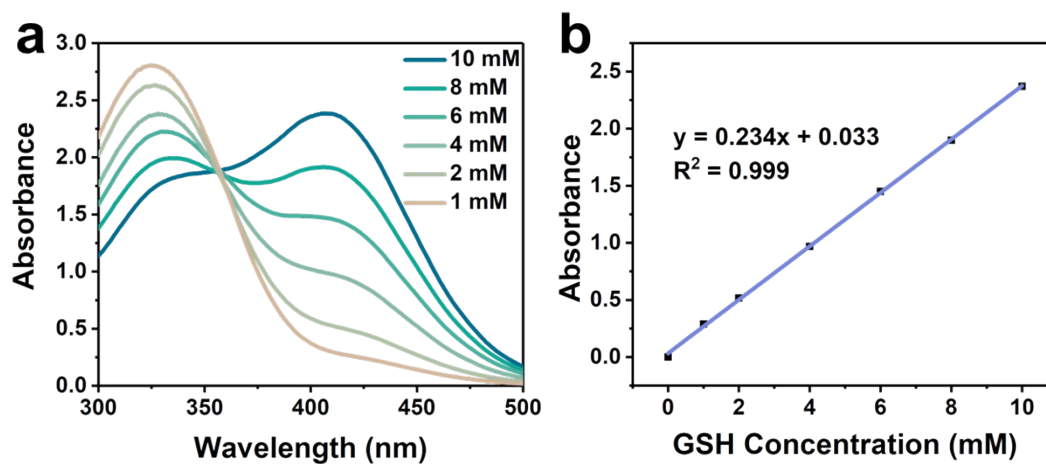


Figure S9. GSH standard curve. (a) UV-vis absorption spectra of the DTNB solution after the reaction with GSH at various concentrations. (b) The linear relationship between the absorbance at 412 nm and concentration of GSH.

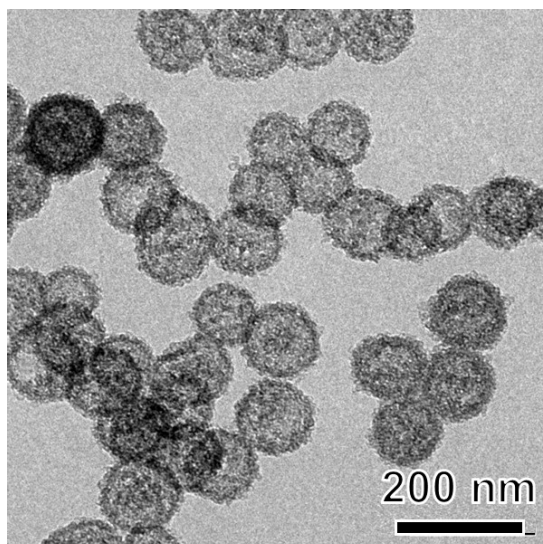


Figure S10. TEM image of HMSNs.

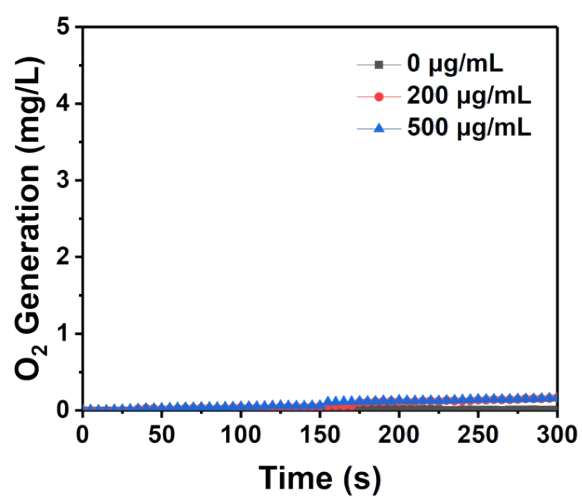


Figure S11. O_2 production by MSNAs-TPP with varied concentration in H_2O_2 solutions.

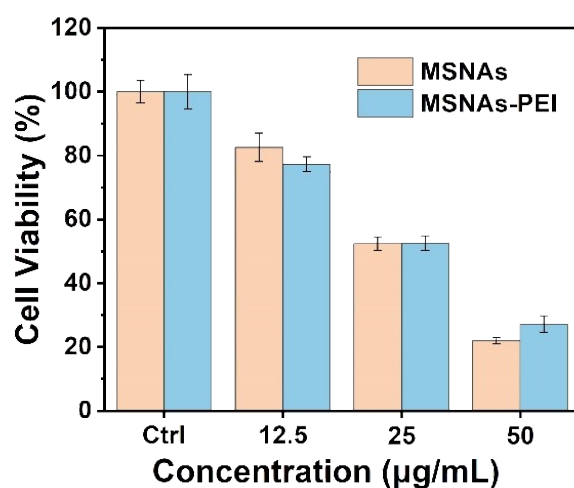


Figure S12. Cell viabilities of 4T1 cells after incubation with various concentrations of MSNAs and MSNAs-PEI for 24 h (n = 4, mean ± s.d.).

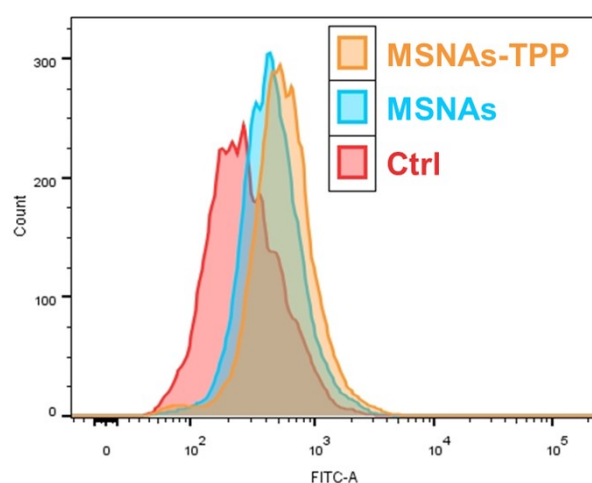


Figure S13. Flow cytometry analysis of ROS in cancer cells after different treatments.

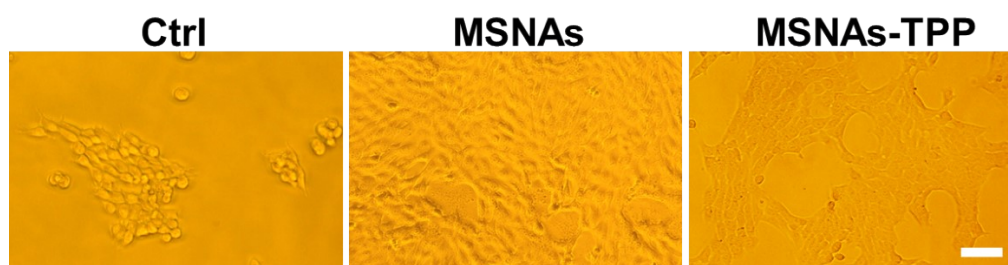


Figure S14. Corresponding bright-field microscopy image of figure 3g. Scale bar is 50 µm.

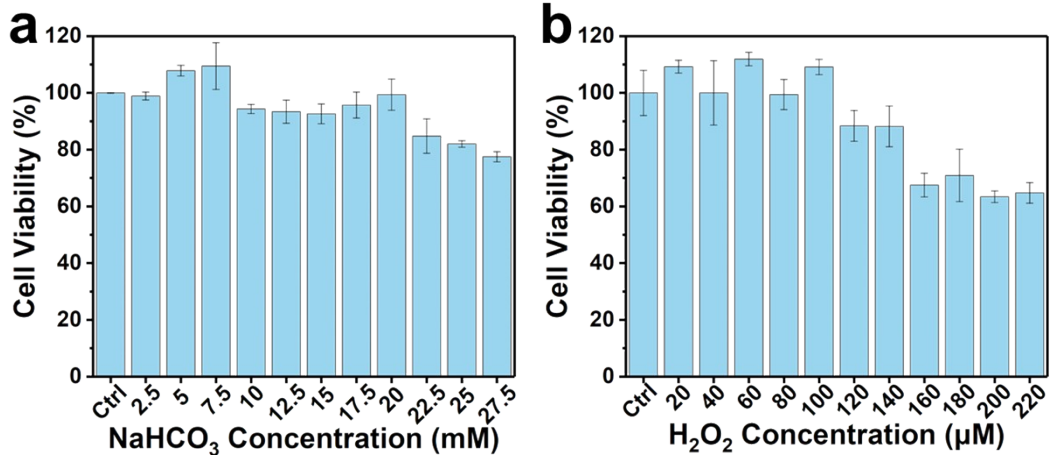


Figure S15. Effect of different concentrations of (a) NaHCO₃ and (b) H₂O₂ on cell viability of 4T1 cells.

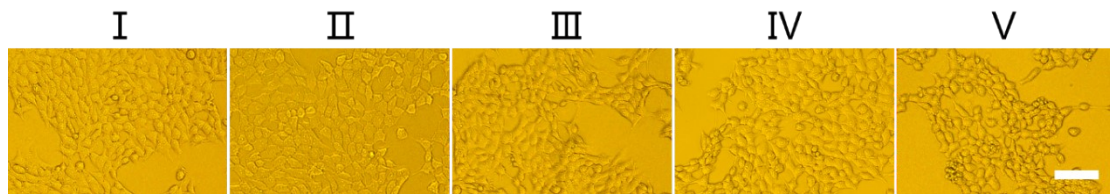


Figure S16. Corresponding bright-field microscopy image of figure 4e. Scale bar is 100 μm.

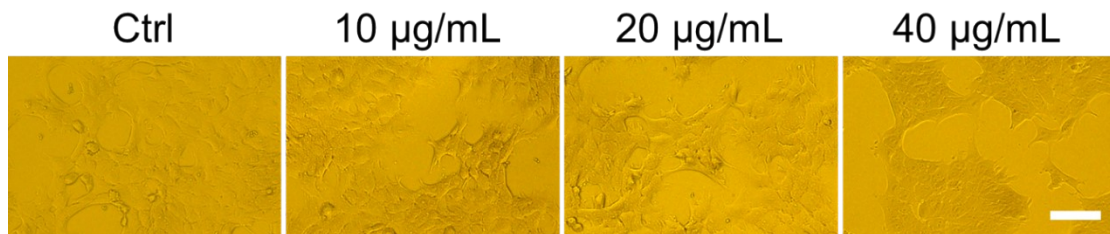


Figure S17. Corresponding bright-field microscopy image of figure 4f. Scale bar is 50 μm.

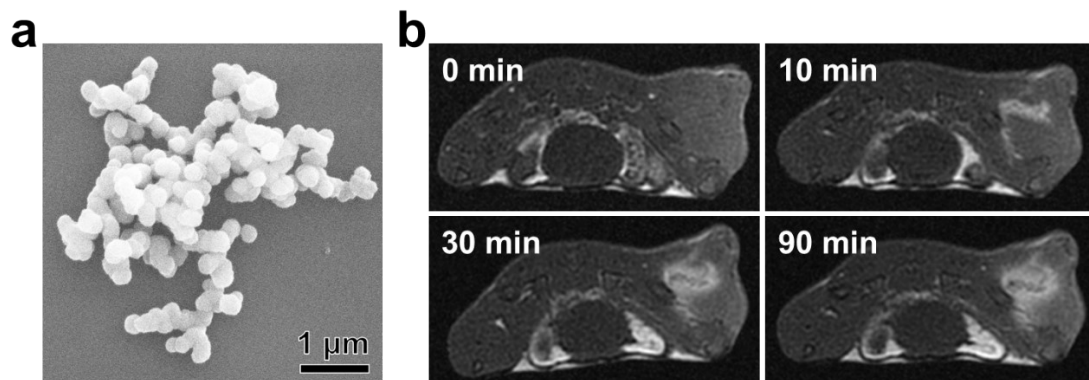


Figure S18. (a) As synthesized MnO₂ nanoparticles. (b) T₁-weighted MR images of 4T1 tumor-bearing mice before and after the intratumor injection of MnO₂ nanoparticles.

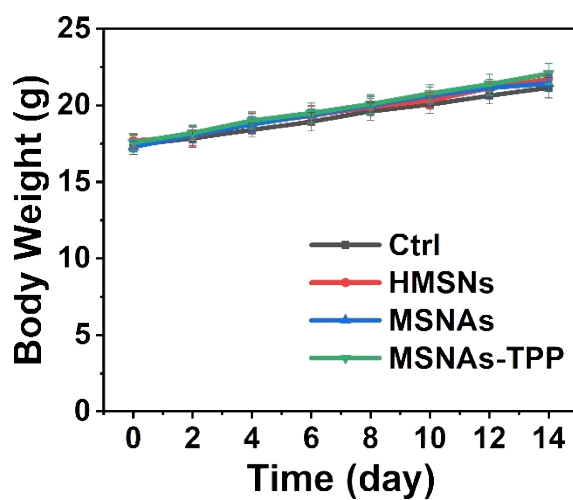


Figure S19. Body weight variation of the mice after different administration. (n = 5, mean ± s.d.)

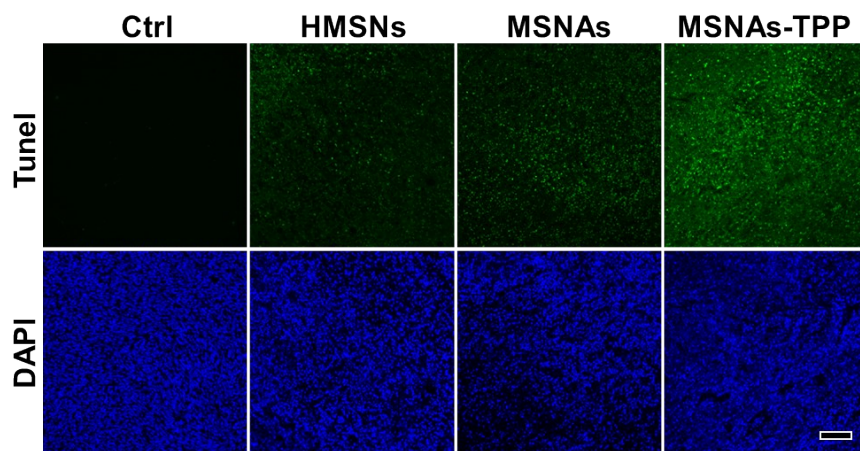


Figure S20. Corresponding tunel and DAPI images of figure 5f. Scale bar is 100 μm.

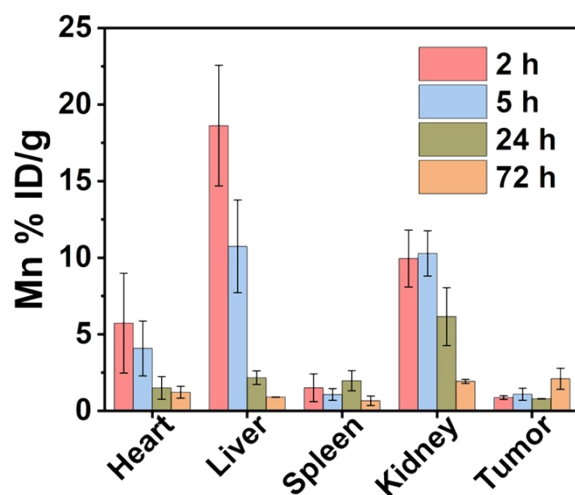


Figure S21. Biodistribution of Mn after intravenous administration of MSNAs-TPP at different time points (n = 3, mean \pm s.d.)

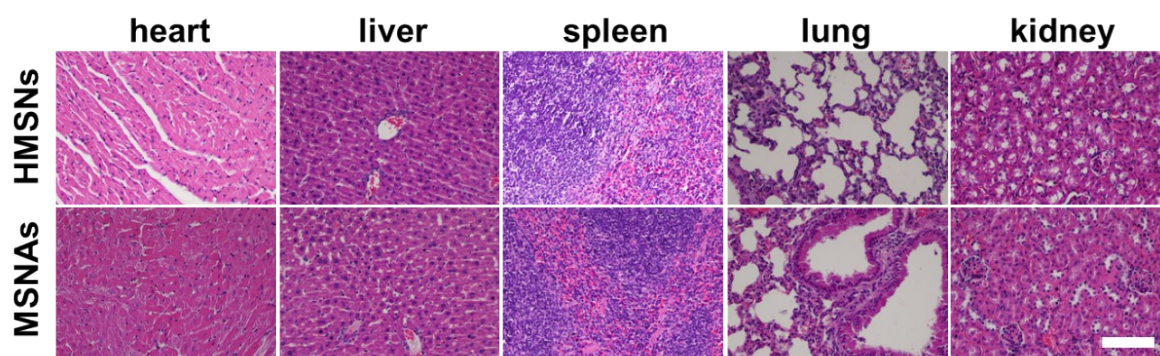


Figure S22. H&E stained images of the major organs (heart, liver, spleen, lung and kidney) of mice collected 2 days after receiving HMSNs and MSNAs treatment. Scale bar is 100 μ m.